Photopyroelectric deconvolution of bulk and surface optical-absorption and nonradiative energy conversion efficiency spectra in Ti:Al_2O_3 crystals

J. Vanniasinkam, A. Mandelis, and S. Buddhudu
Photothermal and Optoelectronic Diagnostics Laboratory, Department of Mechanical Engineering, University of Toronto, Toronto M5S 1A4, Canada

M. Kokta
Union Carbide, Incorporated, Washougal, Washington 98671

(Received 7 January 1994; accepted for publication 18 February 1994)

The extension of an earlier monolithic photopyroelectric spectroscopic model [A. Mandelis *et al.*, Phys. Rev. B **48**, 6808 (1993)] to include surface and bulk optical absorptions and the subsequent optical-to-thermal (nonradiative) energy conversion efficiencies associated with these sites has allowed the self-consistent determination of visible spectra of these quantities, using a very sensitive noncontact experimental configuration to obtain in-phase and quadrature photopyroelectric spectra of Ti:sapphire crystals of two thicknesses and figures of merit.

I. INTRODUCTION

Very recently lock-in quadrature photopyroelectric spectroscopy (Q-PPES) was used in a novel noncontact experimental scheme to obtain high-resolution spectra of the optical-to-thermal energy conversion efficiency (nonradiative coefficient) $\eta_{NR}(\lambda)$ of Ti:sapphire laser crystals with widely different figures of merit (FOM).[1] Simultaneous optical-absorption coefficient $\beta(\lambda)$ spectra were obtained from the lock-in in-phase (IP) PPES signal, i.e., in the purely optical transmission mode. The IP and Q data were combined self-consistently in a monolithic theoretical model to yield $\beta(\lambda)$ and $\eta_{NR}(\lambda)$ spectra of Union-Carbide-grown crystals of various thicknesses. The theoretical model[1] only allowed the determination of total $\beta(\lambda)$ and $\eta_{NR}(\lambda)$ values, and therefore the spectra were found to depend strongly on sample thickness. It is clear that the observed strong optical absorptions in thin samples (accompanied by high values of η_{NR}) and the respectively low $\beta(\lambda)$ values of thick samples (accompanied by much lower values of η_{NR}) were due to efficient surface absorption and nonradiative surface layers (NRSL), which our monolithic model could not account for quantitatively. When dealing with relatively highly absorbing condensed phases, bulk absorptions usually dominate the effects of NRSLs and contacting PPES may be used successfully to generate optical-to-thermal energy conversion efficiency spectra.[2–4] On the other hand, transparent optical materials require extremely good control of all sources and sinks of heat, in order to produce reproducible and accurate $\eta_{NR}(\lambda)$ spectra, free of experimental artifacts. To satisfy this stringent requirement in the case of Ti:sapphire crystals, we developed the noncontact geometry of Fig. 1 to eliminate the effects of thermal resistance at the sample-detector [polyvinylidene fluoride (PVDF)] interface.[1] The remaining NRSL problem is, however, harder to quantify without a suitable theoretical model to deconvolute its effect from crystal bulk energy conversion. Furthermore, NRSLs are potentially of great interest in Ti:Al_2O_3 crystal growth and surface processing (cutting and polishing) optimization.

In this work the earlier monolithic PPES model applicable to Ti:sapphire crystals[1] was suitably modified to include the effects of surface absorptions in the form of NRSLs. Surface and bulk contributions to PPES signals were deconvoluted from experimental data using two crystals of identical properties and different thicknesses. Strong impact of the signal deconvolution on the resulting $\beta_b(\lambda)$ and $\eta_{NR}^{(b)}\times(\lambda)$ spectra was observed, yielding information on bulk- and surface-dominated spectral regions.

II. THEORY

In the geometry of Fig. 1 the surface reflectance of the pyroelectric PVDF thin film was assumed to be zero, corresponding to a very thin soot layer flame deposited on the detector. In the presence of infinitesimally thin surface layers of absorptance A_s at $x=0$, l, the summation of infinite interreflections at depth x in the crystal yields the optical intensity

$$I(x)=I_0\left(\frac{(1-R_s)e^{-A_s}}{1-R_s^2e^{-2(\beta_b l+2A_s)}}\right)\times(e^{-\beta_b x}+R_s e^{-2A_s-\beta_b(2l-x)}). \tag{1}$$

Therefore, the optical intensity escaping the crystal and impinging on the pyroelectric detector is

$$I_t(l)=I_0\left(\frac{(1-R_s)e^{-(A_s+\beta_b l)}}{1-R_s^2e^{-2(\beta_b l+2A_s)}}\right)(1+R_s e^{-2A_s}). \tag{2}$$

When modulated optical intensity $I_0(\omega;\lambda)=I_0(\lambda)\,e^{i\omega t}$ is incident on the crystal at $x=0$, the following coupled thermal-wave equations in the air g, solid s, and pyroelectric p must be solved:

$$\frac{d^2T_g}{dx^2}-\sigma_g^2T_g=0, \quad x\leq 0 \quad \text{and} \quad l\leq x\leq l+L, \tag{3a}$$

$$\frac{d^2T_p}{dx^2}-\sigma_p^2T_p=0, \quad x\geq l+L, \tag{3b}$$

$$\frac{d^2T_s}{dx^2}-\sigma_s^2T_s=-\eta_{NR}^{(b)}(\lambda)\beta_b(\lambda)\left(\frac{I(x;\lambda)}{2k_s}\right), \quad 0\leq x\leq l. \tag{3c}$$

In Eqs. (3) $\sigma_j(\omega)\equiv(1+i)\sqrt{\omega/2\alpha_j}$ is the complex thermal diffusion coefficient in the spatial region j with thermal

 0021-8979/94/75(12)/8090/8/$6.00

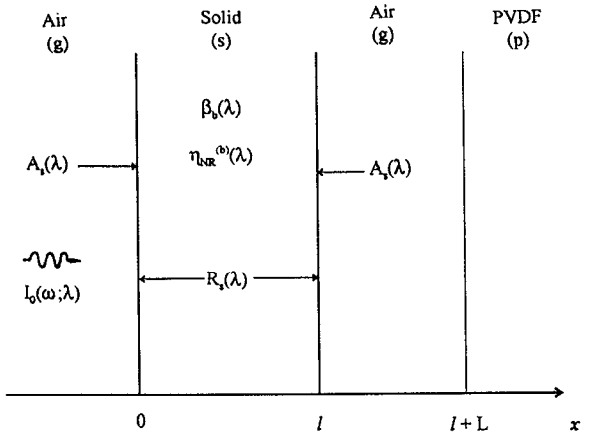

FIG. 1. Schematic of experimental geometry for the modified theoretical analysis of noncontact PPES of a transparent sample of thickness l, bulk optical-absorption coefficient $\beta_b(\lambda)$, bulk nonradiative energy conversion efficiency $\eta_{NR}^{(b)}(\lambda)$, surface absorptance $A_s(\lambda)$, and reflectance $R_s(\lambda)$. Sample thickness: l; airgap thickness: L; and a semi-infinite PVDF detector is assumed. Optical modulation angular frequency: ω; incident optical intensity: I_0.

diffusivity α_j; j: (g,s,p). k_s is the thermal conductivity of the crystal. $I(x;\lambda)$ is given by Eq. (1). The foregoing equations have solutions with integration constants coupled through the boundary conditions of temperature continuity (the result of the absence of interfacial thermal resistances) and heat flux discontinuities (the results of the presence of infinitesimally thin absorbing surface layers) at $x=0$, l. To formulate the heat flux conservation equations, the thermal-wave equation (3c) is rearranged and integrated over a surface layer of thickness ϵ,

$$k_s\int_0^{\epsilon}\left(\frac{d^2T_s(x)}{dx^2}\right)dx - i\rho_s c_s\omega\int_0^{\epsilon}T_s(x)dx = -\frac{1}{2}\,\eta_{NR}^{(\epsilon)}\beta_{\epsilon}\int_0^{\epsilon}I(x;\lambda)dx. \tag{4}$$

Here $\rho_s(c_s)$ is the crystal density (specific heat). Upon integrating and taking $\lim_{\epsilon\to 0}$ of both sides of Eq. (4) using Eq. (1) we obtain

$$-k_s\left.\frac{dT_s(x)}{dx}\right|_{x=0} + k_g\left.\frac{dT_g(x)}{dx}\right|_{x=0} = \frac{I_0}{2}\,\eta_{NR}^{(0)}A_s\left(\frac{(1-R_s)(1+R_se^{-2A_s})}{1-R_s^2e^{-2(\beta_b l+2A_s)}}\right), \tag{5}$$

where, by definition:

$$A_s \equiv \lim_{\epsilon\to 0}(\beta_{\epsilon}\epsilon) \tag{6}$$

and

$$\eta_{NR}^{(0)} \equiv \lim_{\epsilon\to 0}\eta_{NR}^{(\epsilon)}. \tag{7}$$

Similarly, if Eq. (3c) is integrated between $l-\epsilon$ and l and $\lim_{\epsilon\to 0}$ is taken of both sides, it yields

$$k_s\left.\frac{dT_s(x)}{dx}\right|_{x=l} - k_g\left.\frac{dT_g(x)}{dx}\right|_{x=l} = \frac{I_0}{2}\,\eta_{NR}^{(0)}A_s\left(\frac{(1-R_s)(1+R_se^{-2A_s})}{1-R_s^2e^{-2(\beta_b l+2A_s)}}\right)e^{-\beta_b l}, \tag{8}$$

where it was assumed by symmetry that

$$\lim_{\epsilon\to l}[\beta_{l-\epsilon}(l-\epsilon)] = A_s \tag{6'}$$

and

$$\lim_{\epsilon\to l}\eta_{NR}^{(l-\epsilon)} = \eta_{NR}^{(0)}. \tag{7'}$$

Equations (5) and (8) replace the heat flux continuity boundary conditions used in Ref. 1, while the heat flux discontinuity at $x=l+L$ (air-pyroelectric interface) becomes

$$-k_p\left.\frac{dT_p(x)}{dx}\right|_{x=l+L} + k_g\left.\frac{dT_g(x)}{dx}\right|_{x=l+L} = I_t(l), \tag{9}$$

with $I_t(l)$ given by Eq. (2). Following the method of Ref. 1 we finally obtain a modified expression for the photopyroelectric voltage $V(\omega)$,

$$V(\omega;\lambda) = [S(\omega)/\sigma_p(\omega)]C(\omega;\lambda), \tag{10}$$

where $S(\omega)$ is an instrumental factor which can be normalized out experimentally when all spectroscopy is carried out at a fixed modulation angular frequency $\omega = 2\pi f$. The factor $C(\omega;\lambda)$ contains all physical and spectroscopic information,

$$C(\omega;\lambda) = \frac{I_0}{k_p\sigma_p(1+b_{gp})}\left(\frac{1-R_s}{1-R_s^2e^{-2(\beta_b l+2A_s)}}\right)\left\{(1-R_s)\left(\frac{1-\gamma_{gs}Ze^{-2\sigma_g L}}{1-\gamma_{gs}\gamma_{gp}Ze^{-2\sigma_g L}}\right)e^{-(\beta_b l+2A_s)}\right.$$
$$+\frac{b_{gs}e^{-(\sigma_s l+\sigma_g L)}}{(1+b_{gs})(1-\gamma_{gs}^2e^{-2\sigma_s l})(1-\gamma_{gs}\gamma_{gp}Ze^{-2\sigma_g L})}\left[\frac{\eta_{NR}^{(b)}\beta_b e^{-A_s}}{\sigma_s(r_s^2-1)}\left(\frac{2}{1+b_{gs}}[r_s(1-R_se^{-2(\beta_b l+A_s)})\right.\right.$$
$$\left.+b_{gs}(1+R_se^{2(\beta_b l+A_s)})]-\{[1+R_se^{-2A_s}+r_s(1-R_se^{-2A_s})]e^{\sigma_s l}-\gamma_{gs}[1+R_se^{-2A_s}-r_s(1-R_se^{-2A_s})]e^{-\sigma_s l}\}e^{-\beta_b l}\right)$$
$$\left.+\eta_{NR}^{(0)}A_s\left(\frac{2}{1+b_{gs}}(1+R_se^{-2(\beta_b l+A_s)})-(1+R_se^{-2A_s})(e^{\sigma_s l}+\gamma_{gs}e^{-\sigma_s l})\right)\right\}. \tag{11}$$

In Eq. (11) the various symbols have their conventional definitions, i.e., k_j is the thermal conductivity of the spatial region j, b_{ij} is the thermal wave coupling coefficient at the interface (i,j),

$$b_{ij} \equiv \frac{k_i \sqrt{\alpha_j}}{k_j \sqrt{\alpha_i}} . \tag{12}$$

Also,

$$\gamma_{ij} \equiv \frac{1-b_{ij}}{1+b_{ij}} , \tag{13}$$

$$r_s \equiv \beta_b / \sigma_s(\omega), \tag{14}$$

and

$$Z \equiv \frac{1-e^{-2\sigma_s l}}{1-\gamma_{gs}^2 e^{-2\sigma_s l}} . \tag{15}$$

It can be seen that while the entire structure of Eq. (11) is affected by the surface absorptance A_s, it is only the last term that includes the effect of the presence of NRSLs at both sample surfaces, through $\eta_{\mathrm{NR}}^{(0)}$. If $A_s=0$, the monolithic expression for the PPE signal in terms of total (lumped) $\beta(\lambda)$ and $\eta_{\mathrm{NR}}(\lambda)$ values [Eq. (11) in Ref. 1] is retrieved immediately, as expected. Other important limits of Eq. (11) are as follows.

(i) The optical transmission mode ($L \to \infty$). In this case considerable simplification occurs,

$$C_\infty(\omega;\lambda) = \frac{I_0}{k_p \sigma_p (1+b_{gp})} \left(\frac{(1-R_s)^2}{1-R_s^2 e^{-2(\beta_b l + 2A_s)}} \right) e^{-(\beta_b l + 2A_s)} . \tag{16}$$

(ii) Absence of a solid layer ($l=0$),

$$C_R(\omega;\lambda) = \frac{I_0(\lambda)}{k_p \sigma_p (1+b_{gp})} . \tag{17}$$

The dependence $I_0(\lambda)$ has been explicitly stated to indicate the importance of this equation as a normalizing (reference) state of spectroscopic experiments.

The combination of Eqs. (16) and (17) yields the total sample absorptance in terms of the normalized PPE signal $V_\infty(\lambda)$,

$$\beta_b l + 2A_s = -\ln\left(\frac{(1-R_s)^2}{2R_s^2 V_\infty} \left\{ \left[1 + \left(\frac{2V_\infty R_s}{(1-R_s)^2} \right)^2 \right]^{1/2} - 1 \right\} \right), \tag{18a}$$

where

$$V_\infty(\lambda) \equiv C_\infty(\omega;\lambda)/C_R(\omega;\lambda). \tag{18b}$$

III. SPECTROSCOPY

A. Optical absorptance

The Ti:sapphire crystals used in this work were grown by the Czochralski pulling technique at Union Carbide. Details of the growth and postgrowth processing have been given elsewhere.[1] The samples examined photopyroelectrically were two pairs of crystals with figure of merit (FOM) of 40 and 800, respectively. FOM is defined as the absorption ratio at 490 and 820 nm. Each pair included a long and a short crystal, both cut from the same rod. All four crystals were subjected to the same surface polish treatment. The reflectance spectra of the Ti:sapphire crystals were recorded (Fig. 2) and these data were subsequently used as $R_s(\lambda)$ in the analysis of the PPE spectra. Noncontact PPE spectra were obtained using the previously described spectrometer[1] (Fig. 3). Optical transmission spectra were obtained from the IP-PPE signal in the purely optical mode. This signal is more than two orders of magnitude stronger than the Q-PPE (purely thermal wave) mode (Fig. 4). The low level of signal exhibited by the Q-PPE mode is characteristic of very weakly absorbing optical materials and is equivalent to a phase shift in the 0.02°–0.2° range. By comparison, Coufal[5] reported minimum PPE phase shifts in the 0.1°–0.8° range with his thermal wave phase shifter contacting the PVDF detector. As a result of the ultrasmall phase shifts detectable by the present noncontact spectrometer through the Q channel, the contribution of the thermally very efficient NRSL closest to the detector element may dominate bulk heating contributions in some spectral regions and thus the PPES signal requires deconvolution. The dominant optical IP signal in Fig. 4 is essentially equal to the normalized PPES amplitude $V_\infty(\lambda)$. Therefore, normalized transmission data from each crystal pair (thicknesses l_1, l_2) were used in Eq. (17) along with reflectance spectra to obtain a system of two equations with two unknown parameters (β_b,A_s) of the form

$$\beta_b l_1 + 2A_s = S_1 , \tag{19a}$$

$$\beta_b l_2 + 2A_s = S_2 . \tag{19b}$$

Note that the low reflectances exhibited in Fig. 2 may also be neglected, if not available; the committed error will be <10%. Figure 5 shows the results of the optical transmission data deconvolution into bulk and surface absorptances for both sets of samples. The bulk absorptances are typical of the Ti^{3+}:Al_2O_3 system and consist of a broad peak centered around 470 nm with a redshifted shoulder. The peak is due to the $^2T_{2g} \to {}^2E_g$ transition broadened by phonons. The shoulder is the result of the Jahn–Teller splitting of the ^2E_g state.[6] An important effect of the bulk/surface absorptance deconvolution is the observation that the bulk spectrum of the FOM=800 crystals becomes essentially zero below 640 nm and the surface absorption completely dominates the optical behavior of these materials. For the FOM=40 crystals the overall bulk absorption is stronger than in the FOM=800 samples; specifically, below 640 nm, bulk and surface absorptances of the thick crystal are of equal strengths, with the bulk absorptance of the FOM=40 sample being considerably larger than that of the FOM=800 in the same spectral region. On the other hand, the 400–600 nm range is almost completely dominated by the bulk absorptions in the thick crystals, while the thin crystals are dominated by surface effects throughout the entire visible range examined in this work. The high optical quality of the FOM=800 crystal bulk seems to be seriously compromised by the dominant surface ab-

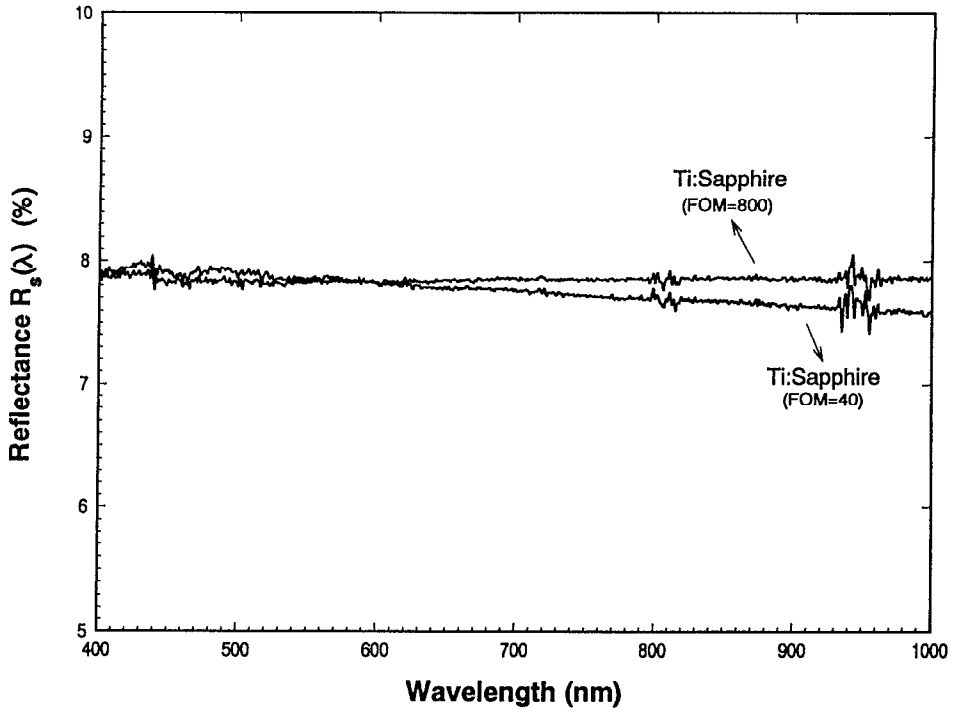

FIG. 2. Reflectance spectra $R_s(\lambda)$, of 2.0-cm-thick Ti:sapphire crystals with FOM=40 and 800.

sorptions for $\lambda \approx 620$ nm. Since this region coincides with the fluorescence emission spectrum of Ti^{3+}:Al_2O_3 in the entire 10–300 K range,[7] Fig. 5(b) indicates that greater care of the surface polishing treatment of laser rods must be taken than in the current technologies, which mainly focus on improvements of the bulk crystal quality.[8] In terms of bulk absorption coefficient spectra, the lower overall $\beta_b(\lambda)$ of the FOM =800 crystals is consistent with improved optical quality. This is the result of one additional annealing (in pure H_2 at 1940 °C for 180 h) of these crystals out of the original batch in which all our materials originated.[8] In Fig. 5(a) the bulk absorption cross section of the FOM=800 crystals becomes zero at $ca \sim 640$ nm, in agreement with the minimum photon energy threshold required to induce a $^2T_{2g} \rightarrow {}^2E_g$ electronic transition [~6471 Å (Ref. 7)]. The near-IR bulk absorption of the FOM=40 ("unannealed") crystals is intrinsic to Czochralski-grown crystals and has been associated with Ti^{3+} ions in interstitial or defect sites close to native defects.[8] A different school of thought proposed that pairs of Ti^{3+}-Ti^{4+} ions are responsible,[6] based on observations of pair-related absorption in solutions.[9]

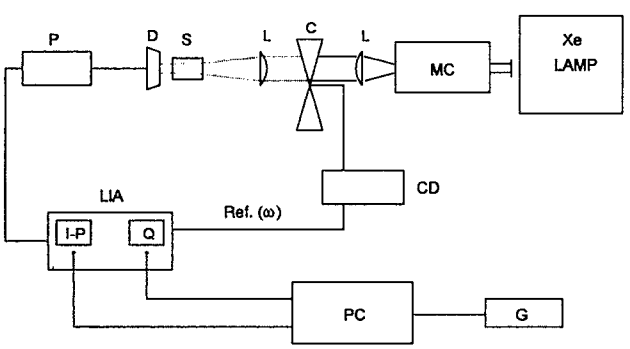

FIG. 3. Schematic of noncontact PPES apparatus. MC: monochromator; L: lens; C: chopper; S: sample; D: detector; P: preamplifier with adjustable bandpass filters; LIA: lock-in amplifier (EG&G model 5210 in IP and Q mode); CD: chopper driver; PC: computer for data acquisition, processing and theoretical analysis; G: graphics and plotter.

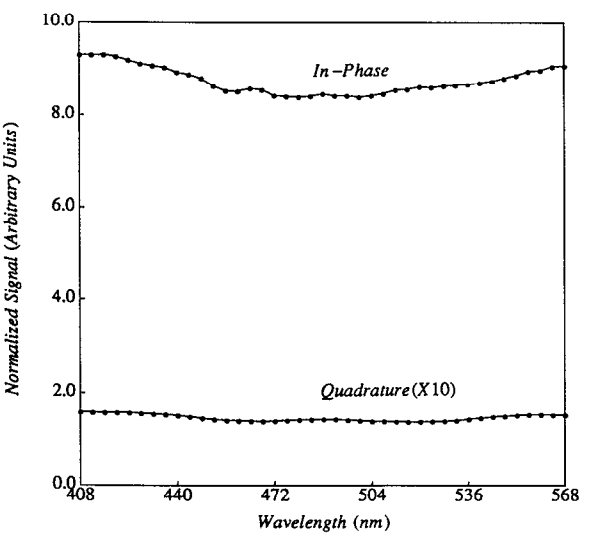

FIG. 4. In-phase (IP) and quadrature (Q) spectral signal levels from a thin Ti:sapphire disk (FOM=40), normalized by the lamp (reference) spectrum at $f=9$ Hz. Sample detector separation in Q-PPE mode: 200 μm.

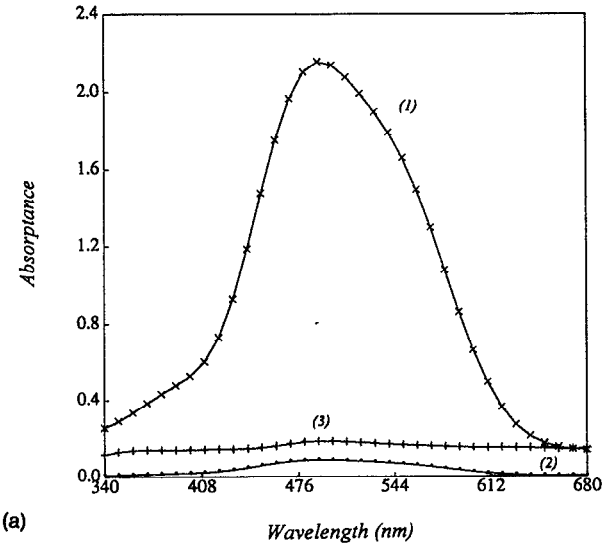

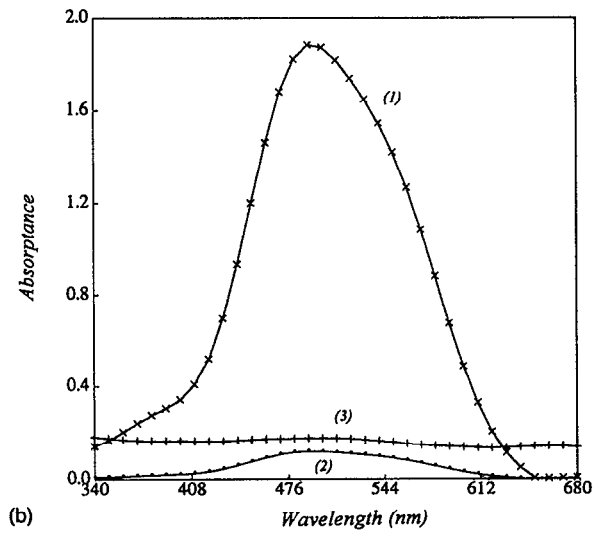

FIG. 5. Optical-absorptance spectra of Ti^{3+}: Al_2O_3 crystals, obtained with PPES in the purely optical transmission mode at $f=9$ Hz, Eq. (17); (a) FOM=40, $l_1=2.017$ cm, and $l_2=0.081$ cm; (b) FOM=800, $l_1=2.013$ cm, and $l_2=0.1295$ cm. Curve labels: (1) $\beta_b l_1$; (2) $\beta_b l_2$; (3) $2A_s$.

A comparison between the present PPES theoretical treatment and the earlier monolithic one[1] in terms of their effects on the purely optical (IP) signal can be assessed from Fig. 6. The most important disadvantage of the monolithic theory is its assignment of the subthreshold absorption to bulk effects. In the absorption range (340–620 nm) it tends to overestimate $\beta(\lambda)$ by ~10% for both sets of crystals. It is seen below that much more dramatic underestimates of the nonradiative energy conversion coefficients were obtained with the monolithic PPES treatment.[1]

B. Optical to thermal energy conversion efficiency

Thermal energy generation spectra were recorded after the $L\rightarrow\infty$ (purely optical) measurements were performed, by decreasing the distance L to some predetermined value <1 mm, at which a measurable, stable, and reproducible quadrature signal was present. The quadratures of the PPES signals corresponding to "infinite" and finite L distances were subtracted at each wavelength. An accurate estimate of the absolute L value for each Q signal corresponds to

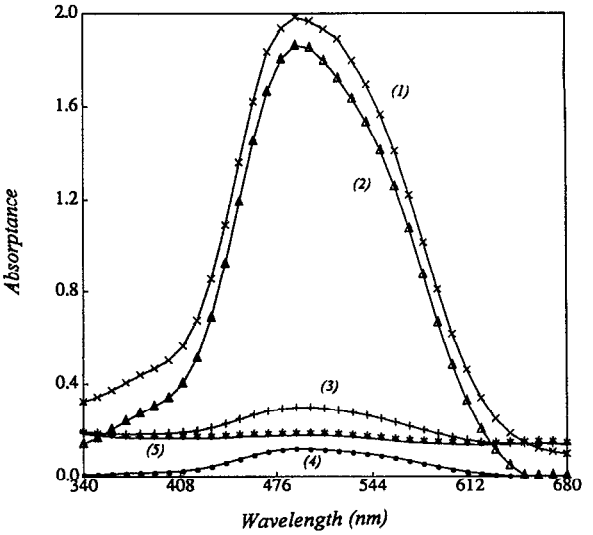

FIG. 6. Comparison between absorptance deduced from the monolithic PPES theory [Eq. (15), Ref. 1] and the present, modified treatment [Eqs. (18)], for the FOM=800 samples. Curve labels: (1) $\beta_m l_1$; (2) $\beta_b l_1$; (3) $\beta_m l_2$; (4) $\beta_b l_2$; (5) $2A_s$. β_m denotes the total absorption coefficient measured using the monolithic theory. Similar effects were observed with the FOM=40 crystal.

$$S_Q(\omega;\lambda)\equiv \mathrm{Im}[C_L(\omega;\lambda)/C_R(\omega;\lambda)]. \tag{20}$$

An additional simplification made in Ref. 1 was the (then numerically justified) neglect of the imaginary part of the first term in the right-hand-side brackets of Eq. (11). This term represents direct optical transmission and is essentially real: the Z-dependent ratio in the parentheses is ≈ 1, correct to order $\delta_{gp}(2-\delta_{gp})=1.9\times10^{-2}$, where[1] $\delta_{gp}\equiv 1-\gamma_{gp}$. The small imaginary part of the Z-dependent ratio originates in the spatial interference pattern (infinite interreflections) of thermal waves trapped between the back surface of the sample at $x=l$, and the pyroelectric detector surface at $x=l+L$. Since the aforementioned correction factor due to this term is on the order of 10^{-2}, the same as the relative ratio of Q and IP signals, a further investigation of its presence showed that the lowering of β_b values expected with the modified PPES theory (Fig. 6) might have a non-negligible effect at the wings of the central Ti:sapphire absorption band. Therefore, it was decided to keep the term in question in our calculations of Eq. (20). To ascertain that the PPE instrument was capable of producing realistic absolute $\eta_{NR}(\lambda)$ spectra, a test Si wafer sample was used, with a thin layer of soot on the polished surface facing the monochrometer. Under these conditions the PPE signal, Eq. (11), can be considerably simplified using entirely bulk absorption:

$$e^{-\beta_b l}\simeq 0, \quad |r_s|\gg 1, \quad A_s=0, \quad R_s=0.$$

The final expression for $C(\omega)$ yields the photothermally saturated signal,

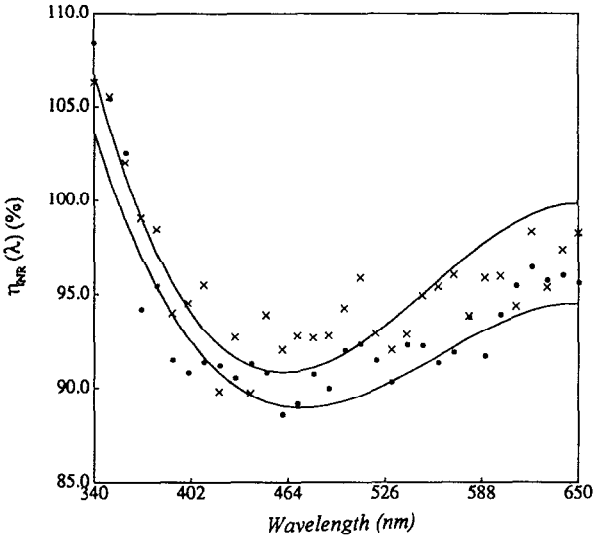

FIG. 7. Optical to thermal energy conversion efficiency spectrum of a sooted Si wafer using normalized Q-PPES. Data points were obtained using two successive experiments (to check reproducibility) in the 380–650 nm range (to check spectral constancy/deviation from the theoretical 100% level). The curves are fourth-order polynomial fits to each set of data.

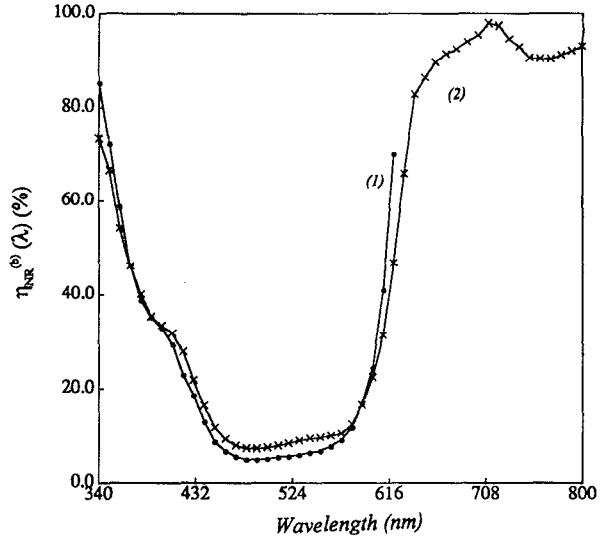

FIG. 8. Optical to thermal energy conversion efficiency spectra of the two pairs of Ti^{3+}: Al_2O_3 crystals. FOM=40 samples, curve (1); FOM=800 samples, curve (2). Each curve was generated from combined Q-PPES data and IP-PPES-determined β_b and A_s spectra from a pair of equal FOM crystals.

$$C_L(\omega)=\frac{2I_0 b_{gs}}{k_p\sigma_p(1+b_{gp})(1+b_{gs})^2}\,\eta_{NR}^{(b)}\left(\frac{e^{-\sigma_s l}}{1-\gamma_{gs}^2 e^{-2\sigma_s l}}\right)\times\left(\frac{e^{-\sigma_g L}}{1-\gamma_{gs}\gamma_{gp}e^{-2\sigma_g L}}\right), \tag{21a}$$

$$\equiv \eta_{NR}^{(b)} F(\omega,l,L,\alpha_s,\gamma_{gs}\gamma_{gp}). \tag{21b}$$

For the sooted Si wafer $\eta_{NR}^{(b)}$ is expected to be uniformly 100% throughout the entire spectral region of interest. Equation (20) was used to normalize the Q-PPES data and the $\eta_{NR}(\lambda)$ spectrum obtained quantitatively from Eq. (21) is shown in Fig. 7. Curves from two successive experiments are shown, which indicate 100%±3% variance in the reproducibility of the obtained η_{NR} values, with ±6% nonconstancy across the 380–650 nm range. These spectral variances were deemed characteristic of the accuracy of the PPE spectrometer in producing quantitative optical to thermal energy conversion efficiency spectra; they are clearly much smaller than the large spectral variations observed with the Ti:sapphire crystals.

To calculate $\eta_{NR}^{(b)}(\lambda)$ spectra for our samples the pairwise common values of $\beta_b(\lambda)$ and $A_s(\lambda)$ were inserted in the normalized Eq. (19). In principle, Eq. (11) shows that a pair of spectra, $\eta_{NR}^{(b)}(\lambda)$ and $\eta_{NR}^{(0)}(\lambda)$, can be calculated from the two Q-PPES spectra corresponding to crystal thicknesses l_1 and l_2. The thermophysical values used in these calculations were:[1] $\alpha_s=0.106$ cm^2/s; $k_g=2.38\times10^{-4}$ W cm^{-1} K^{-1}; and $\alpha_g=0.19$ cm^2/s. These values yielded $b_{gs}\approx5.4\times10^{-4}$; and $\gamma_{gs}=0.9989$. Similarly we used[10] $b_{gp}\approx9.76\times10^{-3}$ and $\gamma_{gp}=0.981$.

In practice, it was found that the actual value of $\eta_{NR}^{(0)}(\lambda)$ had little effect on the value of $\eta_{NR}^{(b)}(\lambda)$. Numerical calculations using Eq. (11) were performed by separating out its real and imaginary parts and adopting a polar coordinate representation. The value of $\eta_{NR}^{(0)}(\lambda)$ was henceforth set equal to 1 (=100%) based on physical arguments regarding the damage-originating NRSL. Figure 8 shows $\eta_{NR}^{(b)}(\lambda)$ spectra for the two pairs of crystals, FOM=40, and FOM=800. Curves computed from Q-PPES data obtained from thick and thin crystals are shown for each pair. The deconvolution of surface and bulk processes is seen to produce values of $\eta_{NR}^{(b)}(\lambda)$ quite close to each other. This is a significant improvement over the monolithic theory, which produced differences up to 24% depending on the thickness.[1] Furthermore, the absolute values of the nonradiative energy conversion efficiencies increased; now they stand significantly (~85%) higher than those reported earlier using the monolithic PPES model.[1] The nonradiative efficiencies of each pair of samples increase for $\lambda>490$ nm. The FOM=40 curve attains the ~100% level above 640 nm, and then remains essentially flat. This spectral range coincides with the approximately equal competition between surface and bulk absorption modes, in the FOM=40 spectra, Fig. 5(a). [On absolute $\beta_b(\lambda)$ scale, both thick and thin samples have identical optical-absorption coefficients.] This rapid near- and subthreshold rise of $\eta_{NR}^{(b)}$ can thus be attributed to residual absorptions in the crystal not related to the Ti^{3+} electronic optical transition manifold, but are very likely due to bulk, purely nonradiative defects. The steeper increase of the $\eta_{NR}^{(b)}$ spectra corresponding to the FOM=800 pair of crystals ("annealed") for $\lambda\geq600$ nm is unbounded at 100% and, therefore, unphysical. The cause of this anomaly is the fact that $\beta_b(\lambda)$ plunges to zero in that wavelength range. Therefore, the computation tries to raise the value of $\eta_{NR}^{(b)}(\lambda)$ to extremely high magnitudes, so that the value of the Q-PPE signal will remain finite and well behaved. The foregoing artifact may be corrected by putting $\eta_{NR}^{(b)}(\lambda\geq600\text{nm})=0$ in Eq. (11), followed by the calculation of the NRSL energy

conversion coefficient as the sole pathway to heat release in these high optical quality samples. Nevertheless, very good agreement exists in the $\lambda<600$ nm range of the $\eta_{NR}^{(b)}(\lambda)$ curves of Fig. 8, which strongly indicates similar energy conversion mechanisms in the crystal bulk. This fact is expected, since the electronic $^2E_g \rightarrow {}^2T_{2g}$ transition normally dominates the optical spectrum of both crystals. The slightly higher $\eta_{NR}^{(b)}$ for the FOM=40 crystal pair is expected since the higher density of bulk nonradiative defect centers in these crystals is capable of inducing enhancement of the nonradiative transition quantum efficiency W_{NR} from the metastable excited state. The effect of this $\eta_{NR}^{(b)} \rightarrow W_{NR}$ increase resulted in visibly lower luminescence of the FOM=40 samples and is expected to produce laser rods with higher lasing threshold pump power. cw laser cavity experiments to correlate these findings are currently under way.

IV. DISCUSSION

The range of $\eta_{NR}^{(b)}$ values reported in this work using the first noncontacting, fixed geometry PPES instrument to obtain simultaneous $\beta_b(\lambda)$ and $\eta_{NR}^{(b)}(\lambda)$ spectra is in agreement with some values reported in earlier literature. Albers, Stark, and Huber[11] used a resistive Wheatstone bridge circuit to measure the heat released by a laser-irradiated Ti:sapphire sample in intimate contact with a positive-temperature-coefficient (PTC) resistor. They monitored the change in the electrical characteristics of the PTC resistor resulting from the heat flux from the sample and they reported radiative quantum efficiencies in the 315–325 K temperature range, consistent with 24%–32% η_{NR} values. These are well within the values of our $\eta_{NR}^{(b)}$ spectra, although no direct comparison can be made because Albers and co-workers did not report the wavelength of the heating laser. Byvik *et al.*[12] determined the quantum efficiency (QE) of Czochralski-grown Ti:sapphire crystals using an all-optical integrating sphere luminescence method. The measured value at 514.5 nm (QE =0.7) implies $\eta_{NR}=30\%$. This is much higher than shown in Fig. 7; however, the integrated luminescence measurements can only estimate a value for the spectrally integrated thermal energy release, unlike the present spectrally distributed values. This fact accentuates the need for wavelength-resolved $\eta_{NR}^{(b)}$ measurements. The optical to thermal energy conversion efficiency values in Ti:sapphire (60% range; 460–510 nm) recently reported by Li, Duncan, and Morrow[13] using a dc thermal technique are, again, too high compared with our values, although their monotonic $\eta_{NR}(\lambda)$ increase with decreasing wavelength is a trend consistent with our spectra. It is important to note, however, that Li and co-workers did not separate out any surface absorptions. These energy release sites, if unaccounted for, would tend to produce phenomenologically higher-than-the-true-bulk η_{NR} values with dc thermal techniques, which do not produce spatially weighted thermal profiles, unlike thermal waves. A more detailed discussion of η_{NR} absolute value artifacts associated with dc heating probes has been given in Ref. 1. On the contrary, Eilers, Hömmerich, and Yen[14] used a pulsed photothermal beam deflection technique and calculated an η_{NR} (532 nm)=13.9% for Ti:Al_2O_3 in good agreement with results in Fig. 8; no further information on the origins of their crystal was given. The foregoing discussion, however, shows how greatly variant η_{NR} calculations are of nominally similar crystals performed by different groups using different methods. It appears that many of the assumptions concerning the calibration of thermal measurement instrumentation associated with optical calorimetry are not adequate and the extent of surface versus bulk contributions to the signal has not been appreciated fully. A pertinent example is the critique made of laser calorimetric methods by Ramponi and Caird.[15]

V. CONCLUSIONS

A modification/extension of the earlier monolithic PPES theory for noncontact spectral characterization of the nonradiative (optical to thermal) energy conversion efficiency in transparent, optical-grade materials has allowed the successful deconvolution of surface and bulk contributions to this quantity in Ti:sapphire crystals as well as of the optical-absorptance spectra. Contributions to the absorption and nonradiative spectra from the polished crystal surfaces, acting as efficient NRSLs, were found to be substantial in the important optical emission range $\lambda \geqslant 600$ nm. This fact strongly suggests that technical attention should be shifted to improving the surface treatment processes, rather than enhancing the bulk optical quality of Ti:sapphire crystals. Both high- and low-figure-of-merit crystal samples from Union Carbide exhibited very similar nonradiative behavior in the optical-absorption range $\lambda<600$ nm, with residual absorptions (perhaps due to bulk defects) below that range producing highly efficient nonradiative energy conversion in the low-FOM samples. No conclusions could be drawn about the high-FOM sample bulk energy conversion pathways in the $\lambda>600$ nm range, owing to the essentially complete transparency of the bulk. The foregoing observations carry important implications for industrial crystal growth and process control, especially with regard to surface treatment (polish) of crystals destined for use as laser rods.

ACKNOWLEDGMENTS

The authors gratefully acknowledge a Strategic Grant from the Natural Sciences and Engineering Research Council of Canada (NSERC), which made this work possible.

[1] A. Mandelis, J. Vanniasinkam, S. Buddhudu, A. Othonos, and M. Kokta, Phys. Rev. B **48**, 6808 (1993).
[2] A. Mandelis, R. E. Wagner, K. Ghandi, R. Baltman, and P. Dao, Phys. Rev. B **39**, 5254 (1989).
[3] C. Christofides, A. Mandelis, K. Ghandi, and R. E. Wagner, Rev. Sci. Instrum. **61**, 2360 (1990).
[4] M. Chirtoc, R. M. Candea, and J. Pelzl, Appl. Spectrosc. **47**, 1071 (1993).
[5] H. Coufal, Appl. Phys. Lett. **45**, 516 (1984).
[6] P. F. Moulton, J. Opt. Soc. Am. B **3**, 125 (1986).
[7] B. F. Gächter and J. A. Koningstein, J. Chem. Phys. **60**, 2003 (1974).
[8] P. Lacovara, L. Esterowitz, and M. Kokta, IEEE J. Quantum Electron. **QE-21**, 1614 (1985).
[9] C. K. Jorgensen, Acta Chem. Scand. **11**, 73 (1957).

[10] A. Mandelis and M. M. Zver, J. Appl. Phys. **57**, 4421 (1985).
[11] P. Albers, E. Stark, and G. Huber, J. Opt. Soc. Am. B **3**, 134 (1986).
[12] C. E. Byvik, A. M. Buoncristiani, S. J. McMurray, and M. Kokta, in *Tunable Solid-State Lasers II*, edited by A. B. Budgor, L. Esterowitz, and L. G. De Shazer (Springer, New York, 1986), pp. 242–246.
[13] Y. Li, I. Duncan, and T. Morrow, J. Lumin. **52**, 275 (1992).
[14] H. Eilers, U. Hömmerich, and W. M. Yen, Opt. Mater. **1**, 311 (1992).
[15] A. J. Ramponi and J. A. Caird, J. Appl. Phys. **63**, 5476 (1988).